AAS 14-441

COMPARISON OF SATELLITE ORBIT TOMOGRAPHY WITH SIMULTANEOUS ATMOSPHERIC DENSITY AND ORBIT ESTIMATION METHODS

Michael A. Shoemaker[*], Brendt Wohlberg[†], Richard Linares[‡], David M. Palmer[§], Alexei Klimenko[¶], David Thompson[‖], and Josef Koller[**]

Satellite orbit tomography is a newly developed method for addressing the Dynamic Calibration of the Atmosphere (DCA). The focus of this paper is a side-by-side comparison with other DCA methods that use the raw tracking measurements and solve simultaneously for the orbit state and parameterized density correction. The main contribution of this work is to test the notion that, in general, an estimator benefits from using raw measurements to solve for the state, in contrast with an estimator that uses intermediate estimated quantities in place of the raw measurements.

INTRODUCTION

The influence of atmospheric drag acceleration model errors on LEO satellite orbit propagation is well known, and much effort has been spent in recent years on improving these models.[1] One research area involves the estimation of corrections to a given density model, i.e. the so-called Dynamic Calibration of the Atmosphere (DCA) methods (pp. 569-570 of Ref. 2). Satellite orbit tomography is a newly developed DCA method, inspired by X-ray computed tomography, for estimating the atmospheric density.[3,4,5] The orbit tomography uses the measured change in specific mechanical energy, and relates that to the specific work acting on the satellite due to drag. Previous work has introduced the method and shown its feasibility with numerical simulations. The focus of the present study is a side-by-side comparison with another method of addressing the DCA problem. The main contribution of this work is to test the notion that, in general, an estimator benefits from using raw measurements to solve for the state, in contrast with an estimator that uses intermediate

[*]Postdoctoral Research Associate, Space Science and Applications (ISR-1), Los Alamos National Laboratory, P.O. Box 1663, Mail Stop D466, Los Alamos, NM.

[†]Scientist, Applied Mathematics and Plasma Physics (T-5), Los Alamos National Laboratory, P.O. Box 1663, Los Alamos, NM.

[‡]Postdoctoral Fellow, Space Science and Applications (ISR-1), Los Alamos National Laboratory, P.O. Box 1663, Mail Stop D466, Los Alamos, NM.

[§]Scientist, Space and Remote Sensing (ISR-2), Los Alamos National Laboratory, P.O. Box 1663, Mail Stop D466, Los Alamos, NM.

[¶]Scientist, Space Science and Applications (ISR-1), Los Alamos National Laboratory, P.O. Box 1663, Mail Stop D466, Los Alamos, NM.

[‖]Scientist, Space and Remote Sensing (ISR-2), Los Alamos National Laboratory, P.O. Box 1663, Mail Stop D466, Los Alamos, NM.

[**]Scientist, Space Science and Applications (ISR-1), Los Alamos National Laboratory, P.O. Box 1663, Mail Stop D466, Los Alamos, NM.

estimated quantities in place of the raw measurements. Furthermore, this work shows a simpler example of the satellite orbit tomography compared with previous work, which allows the overall method to be more easily understood.

Satellite orbit tomography assumes that a separate orbit estimation scheme is in place (e.g. a sequential estimator like an Unscented Kalman filter(UKF)) to process raw tracking measurements and produce estimates of the position and velocity. The tomography then treats these estimated states as input measurements of the change in mechanical energy. In contrast, a simultaneous method uses the tracking measurements and solves simultaneously for the orbit state and parameterized density correction. For example, the U.S. Air Force's High Accuracy Satellite Drag Model (HASDM)[6] uses ground-based tracking measurements of a number of satellites, and uses a weighted least squares differential correction method across all targets that simultaneously solves for the density corrections and a state vector for each target. The HASDM DCA corrections are applied to the exospheric and inflection point temperatures in the vertical temperature profile in the Jacchia-70 empirical density model, and are represented as two separate spherical harmonic expansions.

This research is part of the IMPACT (Integrated Modeling of Perturbations in Atmospheres for Conjunction Tracking) project at Los Alamos National Laboratory (LANL), of which several other related efforts are in progress.[7,8,9]

METHODOLOGY

Because the purpose of this study is to compare different estimation methods, a simpler dynamics model is used than developed previously for the satellite orbit tomography. In Ref.5, a full 3-D model with higher-order Earth gravity, solar radiation pressure, atmospheric drag, and third-body gravitation from the Moon and Sun were considered when introducing the tomography method. Here, the dynamics are restricted to 2-D with only two-body gravitation from the Earth and a simple atmospheric drag model (see Fig. 1):

$$\ddot{\mathbf{r}} = -\frac{\mu}{r^3}\mathbf{r} - \frac{1}{2}\rho s \beta v \mathbf{v} \tag{1}$$

where ρ is the density, α is a scalar correction to the density, $\beta \equiv C_\mathrm{d} A/m$ is the ballistic coefficient containing the satellite's drag coefficient (C_d), drag cross-sectional area (A), and mass (m). The position and velocity vectors are $\mathbf{r} = \begin{bmatrix} x & y \end{bmatrix}^T$ and $\mathbf{v} = \begin{bmatrix} \dot{x} & \dot{y} \end{bmatrix}^T$ The density is modeled with a simple exponential:

$$\rho = \rho_0 \exp \frac{R - r}{H} \ , \tag{2}$$

where $\rho_0 = 3.875 \times 10^{-9}$ kg/m^3, $H = 59.06$ km, R is the Earth radius, and $r = |\mathbf{r}|$. The scalar correction to the density is modeled with a Fourier series as follows:

$$s = \frac{a_0}{2} + \sum_{k=1}^{K} a_k \cos(k\phi) + b_k \sin(k\phi) \tag{3}$$

where ϕ is the geocentric latitude: $\phi = \mathrm{atan}(y/x)$.

ESTIMATORS

Several different UKF implementations are used in this study. Each one uses at least the satellite Cartesian position and velocity vectors for M satellites in their state vectors:

$$\mathbf{X} = \begin{bmatrix} \mathbf{r}_1^T & \mathbf{v}_1^T & \cdots & \mathbf{r}_M^T & \mathbf{v}_M^T & a_0 & a_1 & \cdots & a_K & b_1 & \cdots & b_K \end{bmatrix}^T \tag{4}$$

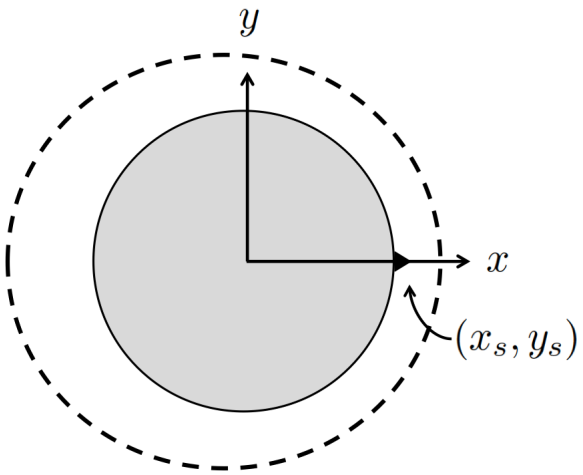

Figure 1. Illustration of 2-D orbit and coordinate system.

We define three different types of UKFs as follows:

- Base UKF, estimating only the Cartesian states for each satellite.
- In addition to the satellite states, estimating a single scalar constant on the density.
- In addition to the satellite states, estimating Fourier series coefficients of degree M.

The full formulation for the UKFs are not repeated here; they can be obtained, e.g. from Ref.10. Although the planned application for the orbit tomography is ground-based angles-only measurements, this study also uses a range measurement. Thus, each satellite i has a measurement vector

$$\mathbf{y}_i = \begin{bmatrix} \delta & d \end{bmatrix}^T \tag{5}$$

where δ is the declination angle measured relative to the local coordinate frame aligned with the xy axes,

$$\delta = \text{atan}(\frac{y - y_s}{x - x_s}) \,, \tag{6}$$

the range is

$$d = \sqrt{(x - x_s)^2 + (y - y_s)^2} \,, \tag{7}$$

and the ground site is specified by coordinates (x_s, y_s).

MOTIVATIONAL EXAMPLE

This section presents a simple example to test our intuition that the UKFs which estimate the density should have less error (*i.e.* bias) in the estimated position and velocity than the UKF which does not estimate the density, but rather uses an *a priori* assumed value for the model (which is slightly in error from truth). Monte Carlo (MC) simulations are performed with 100 runs, assuming a single satellite and a single ground site at $(x_s, y_s) = (R, 0)$. The initial truth state is the same in each run, with a satellite having semi-major axis of 6778 km, eccentricity of 0.001, and all the other Keplerian elements set to zero. In all the examples in this paper, the satellites have the same

assumed values for $A = 1$ m^2, $m = 1000$ kg, and $C_D = 2.2$. The measurements are synthesized from the truth state with 1σ zero-mean additive Gaussian noise of 1 m in range and 10 arcseconds in angle. The satellite's measurements are synthesized such that there are 50 measurements per pass, with 10 sec between measurements, and one pass every orbit. Because this simulation is only concerned with comparing filter outputs, and is not concerned with simulating actual operation of a ground-site, a measurement can take place while the satellite is below the horizon.

Figures 2 and 3 show the resulting error distributions between the final state estimates and the truth state. The means of the position errors in Fig. 2 for each UKF type are also denoted on the figure. It is clear that the simple UKF which only estimates the satellite state has the most bias in the final estimated position. Furthermore, the bias is progressively reduced as the UKFs include more model information in the density. There are slight differences in the variance of the estimates, but these differences are not significant in Figs. 2 and 3.

Thus, this example confirms our intuition that the orbit state estimate improves as higher-fidelity density model parameters are included in the state estimate. Of course, this is a simplified example that does not consider other sources of bias (*e.g.* in the tracking measurements, or in the assumed ballistic coefficient). But the implication is that the previously assumed tomography workflow, in which orbit estimates are treated as the input measurements, would indeed be using slightly biased position and velocity estimates if no density states are also estimated in the UKF. The question that remains, however, is how significant these biases are in the final reconstructed density maps.

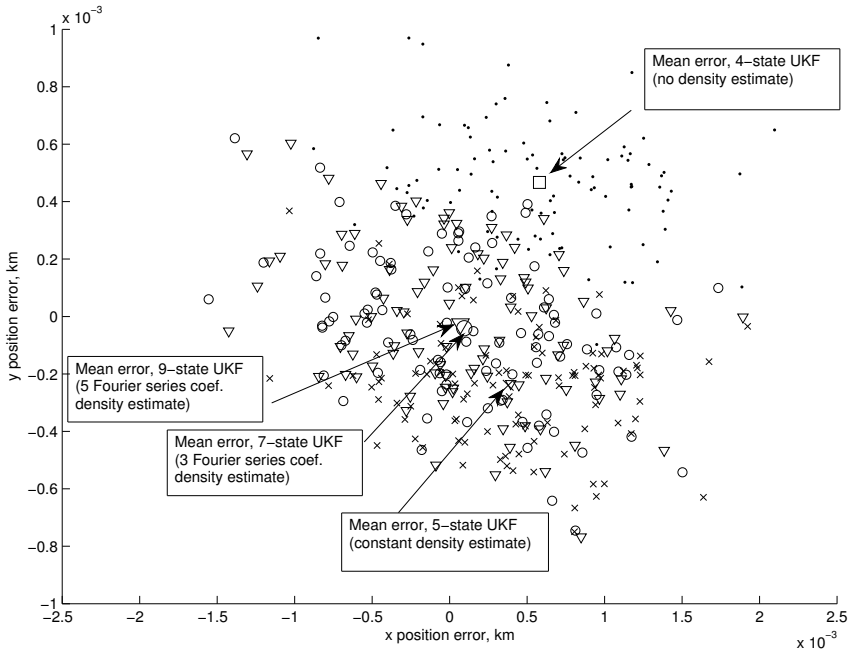

Figure 2. Position error at final measurement time for 100 MC runs, using four different UKFs (see above for description of filters).

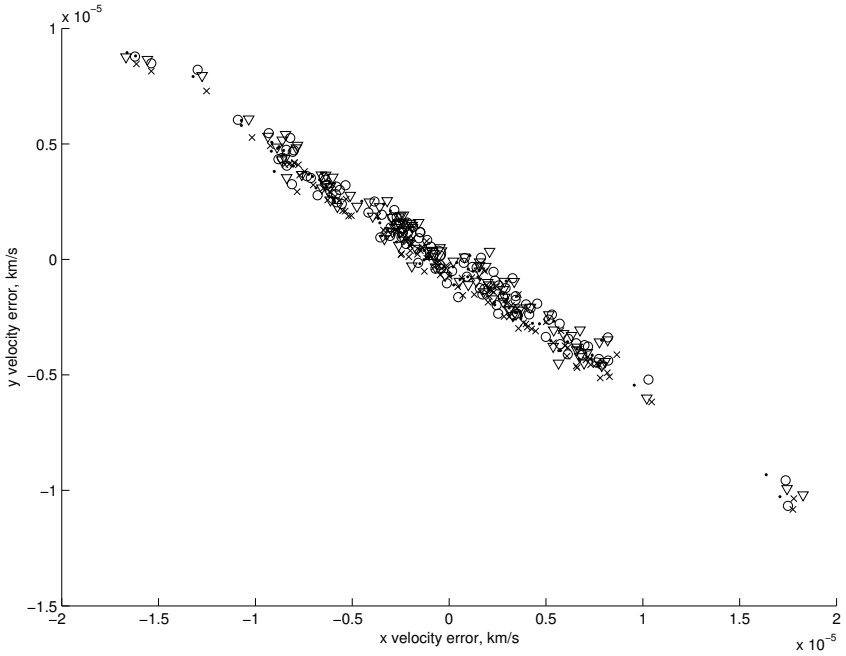

Figure 3. Velocity error at final measurement time for 100 MC runs, using four different UKFs.

COMPARISON WITH TOMOGRAPHY

Using the same simplified 2-D dynamics, we now compare the UKFs described above with the satellite orbit tomography method. The full background and derivation of the tomography formulation is not repeated here because this information can be found in previous publications.[5] The grid is defined in 1-D along ϕ, and the grid spacing is chosen to be $\Delta\phi = 10$ deg (Fig. 4). This simple 2-D case with a 1-D grid allows us to easily describe the gradient operator used in the regularization. As an illustrative example, let the grid contain 4 cells, then the matrix for the gradient operator D would be formed explicitly as

$$\nabla \mathbf{s} = D\mathbf{s} = \begin{bmatrix} -1 & 1 & 0 & 0 \\ 0 & -1 & 1 & 0 \\ 0 & 0 & -1 & 1 \\ 1 & 0 & 0 & -1 \end{bmatrix} \begin{bmatrix} s_1 \\ s_2 \\ s_3 \\ s_4 \end{bmatrix} = \begin{bmatrix} s_2 - s_1 \\ s_3 - s_2 \\ s_4 - s_3 \\ s_1 - s_4 \end{bmatrix} \tag{8}$$

and it is straightforward to extend this formulation to the actual number of cells in $\mathbf{s}$.

In this example, each assumed satellite $i \in \{1, \cdots, M\}$ has an initial Keplerian state described with

$$\begin{bmatrix} a & e & i & \Omega & \omega & \nu \end{bmatrix} = \begin{bmatrix} 6778\text{km} & 1 \times 10^{-3} & 0 & 0 & \omega_i & 0 \end{bmatrix} \tag{9}$$

where the argument of perigee ω_i is chosen such that the $M = 7$ satellites in the present simulation have evenly spaced perigee locations around the 2-D plane. The satellites are simulated with several ground-station passes, each with duration of 500 sec (with 0.1 Hz measurement frequency), with passes occurring once per orbit for 4 orbits, followed by a gap of 6 orbital durations, and then one final pass (Fig. 5). This pass setup is meant to be somewhat representative of the anticipated

application of the tomography method, where the first several passes are used to obtain a good estimate of the position and velocity, and then a gap of several hours (or more) is allowed, after which the next pass is used to again estimate the position and velocity to derive the measured change in mechanical energy. Note, however, the measurements are assumed to be synchronous across all satellites, and thus some satellite "passes" are allowed to occur then the target is below the horizon (*i.e.* a "glass Earth" is assumed). Zero-mean Gaussian measurement noise having 1σ variance of 10 arcsec in the angles and 1 m in the range is added to the synthesized measurements. The UKFs use this same pass setup to process measurements and sequentially estimate the state.

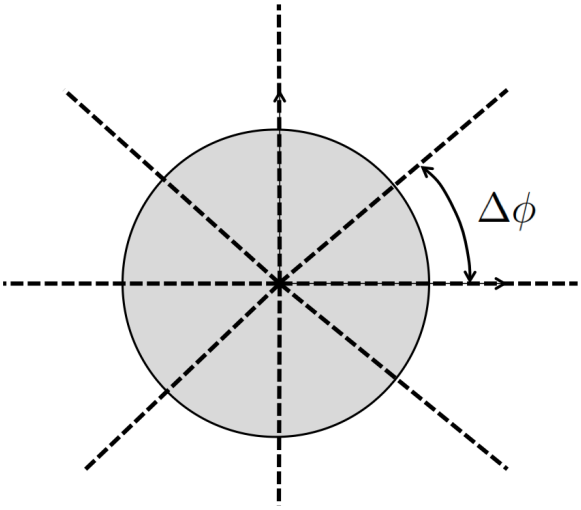

Figure 4. Illustration of 2-D grid.

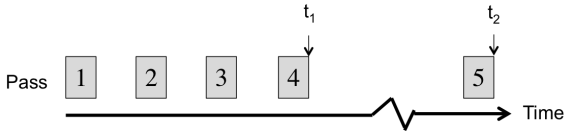

Figure 5. Sketch of assumed pass timing and tomography time span $\Delta t = t_2 - t_1$.

The truth density model in the simulation uses a Fourier series with $K = 3$, where the coefficients are defined as

$$\left[\begin{array}{ccccccc} a_0 & a_1 & a_2 & a_3 & b_1 & b_2 & b_3 \end{array}\right] = \left[\begin{array}{ccccccc} 2.1 & 0.2 & 0.05 & 0.1 & 0.1 & 0 & 0 \end{array}\right] \tag{10}$$

Conversely, the UKFs at most use $K = 2$, and the initial state estimates of these coefficients (where applicable in the given UKF) are defined as

$$\left[\begin{array}{ccccc} \hat{a}_0 & \hat{a}_1 & \hat{a}_2 & \hat{b}_1 & \hat{b}_2 \end{array}\right] = \left[\begin{array}{ccccc} 2.0 & 0.0 & 0.0 & 0.0 & 0.0 \end{array}\right] \tag{11}$$

The initial covariance estimate is populated with the radial and along track position 1σ being 4 m and 78 m, respectively, and the corresponding velocities being 1 cm/s and 10 cm/s. The simulated range and angle measurement noise are the same as above. Each UKF uses an initial state estimate that is constructed by taking the true cartesian state and adding noise sampled from a normal distribution having a variance in each component described by the initial covariance matrix defined above. The

initial state estimate for the density, as defined above in Eq. 11, yields $s = 1.0$ in Eq. 3. The initial covariance estimate for the Fourier series coefficients uses a diagonal matrix with each state on the main diagonal having 1σ variance of 0.1.

Figures 6 and 7 show UKF results at the final measurement time (*i.e.* at the last measurement of pass #5 in Fig. 5). Figure 6 shows the true density profile and that estimated using the UKF with a constant global density scalar. It is not surprising that the estimated constant s is close to the mean of the true s. Figure 7 shows the corresponding plot for the UKF which estimates $K = 2$ Fourier series coefficients, and we see that the estimated $s(\phi)$ profile matches closely with the true value, with a maximum deviation of approximately 20%. Recall that the true profile uses $K = 3$, but we limit the UKF's knowledge of the truth dynamics by only including $K = 2$.

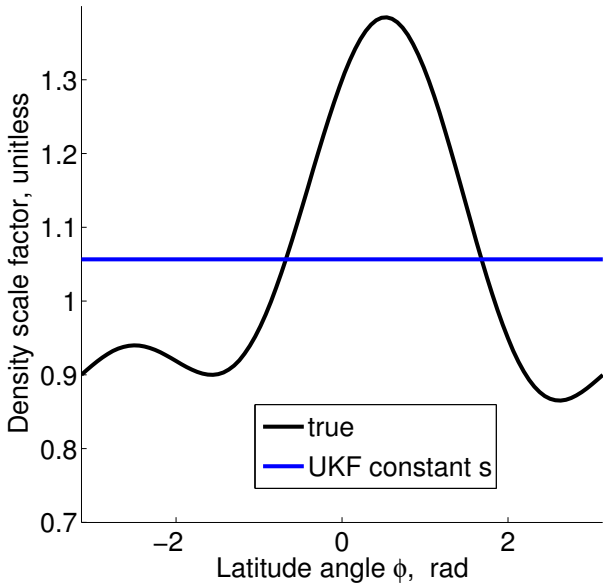

Figure 6. Comparison of truth $s(\phi)$ profile with UKF estimate of profile using constant s (*i.e.* where $K = 0$).

Figure 8 shows the results of running the tomography for two difference cases: one uses the position and velocity estimates generated from the UKF that does not estimate any density information (*i.e* the one which should be most biased, the red line in Fig. 8), as well as one (the blue line in Fig.8) that uses the position and velocity estimates from the UKF that estimates a constant global s (*i.e.* the same one as described in Fig. 6). Two remarks can be made about Fig. 8: (1) The tomography does fairly well at estimating the density profile $s(\phi)$, despite having no inherent modeling of the parameterization. The maximum error in both tomography cases is approximately 0.2, and the mean error is approximately 0.1. (2) The tomography case which uses the position and velocity estimates from the UKF that estimates a constant s global correction (blue line in Fig. 8) has lower error than the tomography case that uses the other UKF outputs (red line in Fig. 8). In other words, the red line in Fig. 8 represents the more biased position and velocity estimates being used in the tomography, compared with the blue line. Thus, this result confirms our intuition that the tomography solution improves if the input position and velocity estimates are less biased.

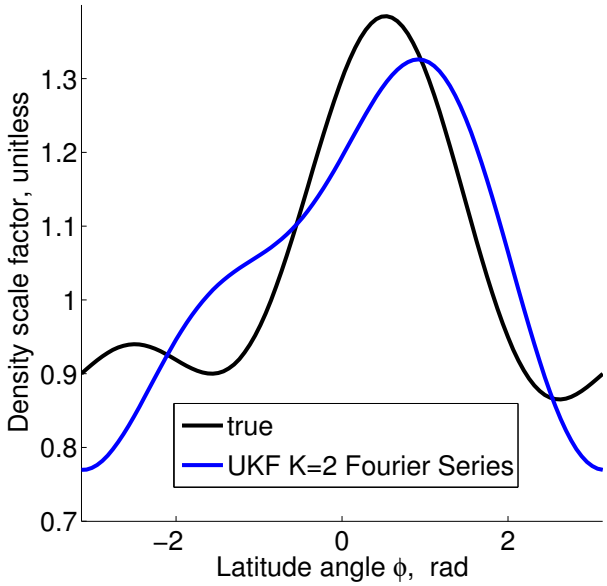

Figure 7. Comparison of truth $s(\phi)$ profile with UKF estimate of profile using $K = 2$.

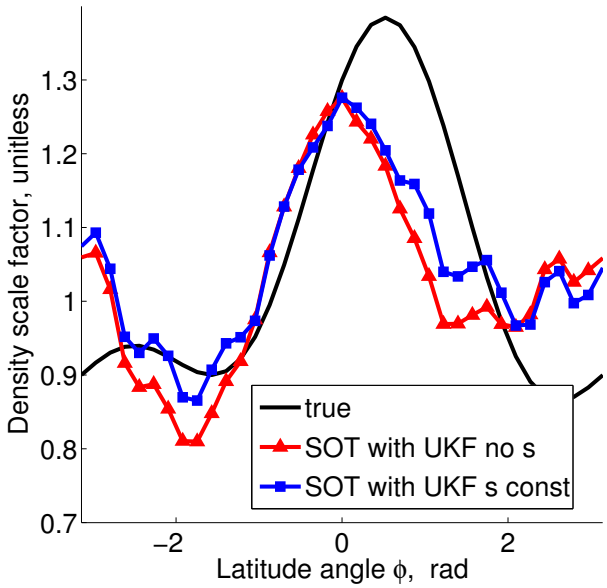

Figure 8. Comparison of truth $s(\phi)$ profile with satellite orbit tomography (SOT) using two different UKF results as input measurements.

DISCUSSION

Another point to consider is the minimum number of satellites required to get an acceptable solution in the tomography method. Figure 9 shows the tomography with the same orbital setup as described above, but with varying number of target satellites, and where the measurements are

perfectly formed from the truth states (*i.e.* the UKFs are not used). Hence, this plot is only concerned with the effect of satellite number on the tomography solution. As can be seen from the plot, as the number of satellites is increased, the tomography solution for the density profile $s(\phi)$ gets closer to truth. Conversely, as the number of satellites is reduced, the quality of the solution degrades as one would expect. However, tests results (which are omitted here) of the UKF with ($K = 2$) and decreasing satellite number, showed that the UKF was better able to estimate $s(\phi)$ with only a few satellites. Thus, an advantage of the tomography method is that it does not require an internal parameterization of the density model, but using a parameterized density model can be advantageous when one is limited to a small set of target satellites (and assuming the parameterization is a good match for the truth density, as assumed in this test). It should be noted that this remark is based on a simplified dynamics scenario in 2-D with a simple density parameterization, thus it remains to be seen if the above remarks hold for a more general case. Lastly, it should be noted that the comparisons above (Figs. 6-8) were restricted to a single simulation run, and thus future work should verify that the same conclusions hold under MC simulations.

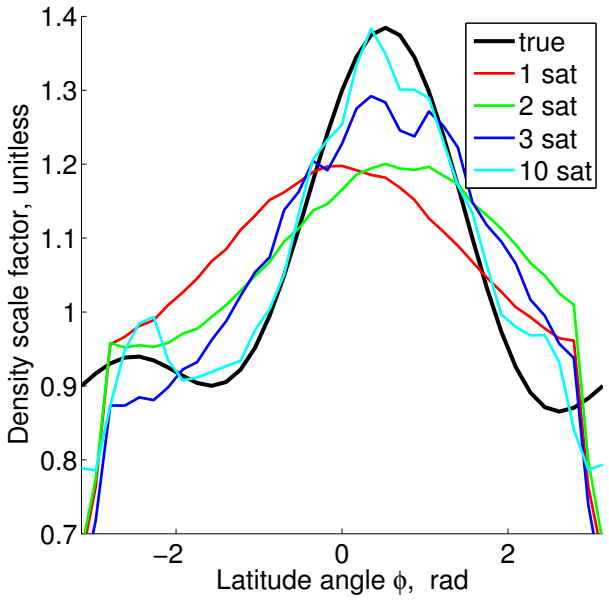

Figure 9. Tomography solution with varying satellite number, assuming perfect measurements.

CONCLUSIONS

This study has presented a simple comparison of satellite orbit tomography with a UKF that estimates both the satellite orbital state and atmospheric density. It was shown that the tomography solution for the density improves slightly when the input position and velocity measurements are less biased, *i.e.* when the pre-tomography UKF estimates a simple constant scalar to the global density, versus not estimating any density information. When comparing the UFK which estimates $K = 2$ Fourier series coefficients to the tomography, the resulting reconstructed density profiles had comparable errors. This result assumed $M = 7$ target satellites. In general, the tomography may be more suitable as the number of target satellites is increased. In contrast, a UKF formulation to solve for both satellite states and the density may be more suitable for a low number of satellites, and if

one is confident in the chosen density model parameterization. Overall, the results in this study are preliminary in nature, since only a simplified 2-D dynamics scenario was considered. Future work should consider more detailed MC simulations.

ACKNOWLEDGMENTS

This work was conducted under the auspices of the U.S. Department of Energy, with support from the Los Alamos National Laboratory (LANL) Directed Research and Development program.

NOTATION

A	drag cross-sectional area, km^2
$\mathbf{a}_d$	drag acceleration vector, km/s^2
a, b	Fourier series coefficients, unitless
C_d	drag coefficient, unitless
D	gradient operator
d	range measurement, km
H	density scale height, km
i	satellite index
K	degree of Fourier series
k	index of Fourier series terms
M	number of satellites
m	mass
R	Earth radius, km
$\mathbf{r}$	position vector of satellite, km
r	magnitude of position, km
$\mathbf{s}$	vectorized density scale factor, unitless
s	density model scale factor, unitless
t	time, s
$\mathbf{v}$	inertial velocity vector, km/s
$\mathbf{x}$	state vector
x_s, y_s	ground site coordinates, km
$\mathbf{y}$	measurement vector
β	drag ballistic coefficient, km^2/kg
δ	declination angle, rad
μ	Earth gravitational parameter, km^3/s^2
ρ	density, kg/km^3
ρ_0	reference density, kg/km^3
ϕ	latitude, rad

REFERENCES

[1] D. Vallado and D. Finkleman, "A critical assessment of satellite drag and atmospheric density modeling," *Acta Astronautica*, Vol. 95, Feb. 2014, pp. 141–165, doi:10.1016/j.actaastro.2013.10.005.

[2] D. A. Vallado, *Fundamentals of Astrodynamics and Applications*. Microcosm Press, El Segundo, California, and Kluwer Academic Publishers, Dordrecht, The Netherlands, third ed., 2007.

[3] M. Shoemaker, B. Wohlberg, and J. Koller, "Atmospheric Density Reconstruction Using Satellite Orbit Tomography," *23rd AAS/AIAA Space Flight Mechanics Meeting, Lihue, Kauai, Hawaii, Feb. 2013*, 2013.

[4] M. Shoemaker, B. Wohlberg, R. Linares, and J. Koller, "Application of Optical Tracking and Orbit Estimation to Satellite Orbit Tomography," *AAS/AIAA Astrodynamics Specialist Conference, Hilton Head, South Carolina, Aug. 2013*, 2013.

[5] M. Shoemaker, B. Wohlberg, and J. Koller, "Atmospheric Density Reconstruction Using Satellite Orbit Tomography," *Journal of Guidance, Control, and Dynamics*, 2014. in press.

[6] M. F. Storz, B. R. Bowman, M. J. I. Branson, S. J. Casali, and W. K. Tobiska, "High accuracy satellite drag model (HASDM)," *Advances in Space Research*, Vol. 36, No. 12, 2005, pp. 2497–2505, doi:10.1016/j.asr.2004.02.020.

[7] J. Koller, "The IMPACT Framework for Enabling System Analysis of Satellite Conjunctions," *24th AAS/AIAA Space Flight Mechanics Meeting, Santa Fe, New Mexico*, 2014. submitted.

[8] A. Walker, M. Shoemaker, P. Mehta, and J. Koller, "Gas-surface Interactions for Satellites Orbiting in the Lower Exosphere," *24th AAS/AIAA Space Flight Mechanics Meeting, Santa Fe, New Mexico*, 2014. submitted.

[9] S. Brennan, "Multi-Model Orbital Simulation Development with Python," *24th AAS/AIAA Space Flight Mechanics Meeting, Santa Fe, New Mexico*, 2014. submitted.

[10] J. Crassidis and J. Junkins, *Optimal Estimation of Dynamic Systems*. Washington, D.C.: Chapman and Hall/CRC, 2004.